Reprinted from The Journal of Physical Chemistry, 1995, 99.

Theoretical Study on the Photochemical Decomposition Reaction of Permanganate Ion, MnO_4^-

Hiromi Nakai, Yutaka Ohmori, and Hiroshi Nakatsuji*,†

Department of Synthetic Chemistry and Biological Chemistry, Faculty of Engineering, Kyoto University, Sakyo-ku, Kyoto 606-01, Japan

Received: November 4, 1994; In Final Form: March 3, 1995[⊗]

The electronic mechanism of the photodecomposition reaction of MnO_4^- is investigated. The symmetry-adapted cluster (SAC)/SAC−configuration interaction (SAC-CI) method is used for calculating the ground and excited states of the permanganate ion along the reaction pathway. Electron correlations are very important for reasonable descriptions of the ground and excited states. The 546- and 311-nm absorption bands, which lead to the photodecomposition reaction, are the dipole-allowed transitions to the 1^1T_2 and 3^1T_2 states, respectively. The lowest excited state plays a key role in the reaction. The decomposition leading to the ground state of the products, $MnO_2^-(^3\Delta_g^+) + O_2(^3\Sigma_g^-)$, occurs directly along the lowest-excited-state potential curve. The energy barrier existing in the lowest-excited-state curve is the origin of the strong wavelength dependence of the quantum yield and the slight temperature dependence at the longer wavelength region observed by Zimmerman (*J. Chem. Phys.* **1955**, *23*, 825). The photochemical and thermal decomposition reactions are shown to be symmetry allowed and forbidden, respectively. The peroxo complex in the 1^1A_1 ground state corresponds to the long-lived intermediate observed experimentally. The electronic mechanism proposed by the present *ab initio* study slightly modifies and confirms the experimental reaction scheme (Scheme 1) given by Lee *et al.* (*J. Am. Chem. Soc.* **1987**, *109*, 3003).

I. Introduction

The permanganate ion, MnO_4^-, in aqueous solution is photochemically decomposed with an evolution of oxygen.[1] Zimmerman[2] measured the quantum yield of oxygen production in the pH range from 6.8 to 13 using light from 254 to 578 nm. The quantum yield strongly depends on the wavelength of the light, slightly on the temperature at the longer wavelength region, and not at all on the composition of the solution or on the light intensity. The shorter wavelength (311 nm) band is much more photoactive than the longer wavelength (546 nm) one. Furthermore, from the isotope experiment he showed that the produced oxygen comes from the permanganate ion and not from the solvent.[2] This result was confirmed by the experiment using rigid glass solutions.[3] Kläning *et al.*[3] showed that atomic oxygens like O and O^- are not produced by this photodecomposition reaction, since hydrogen is not extracted from the solvent alcohols. Furthermore, for the lack of an ESR signal corresponding to the O_2^- anion, they concluded that the photodecomposition reaction proceeds through the formation of a molecular O_2 species as

$$MnO_4^- \rightarrow MnO_2^- + O_2 \qquad (1)$$

Lee *et al.*[4] examined experimentally the photodecomposition process of the permanganate ion and showed an existence of a long-lived, highly oxidative intermediate, which is considered to be the Mn(V) peroxo complex. They proposed a photochemical reaction scheme, Scheme 1, including this intermediate. From the experiments of the quantum yields, they showed that the photooxidizing reactions of several reductants are due to this intermediate rather than the initial excited permanganate, as shown in Scheme 1. Furthermore, by a qualitative molecular orbital consideration, they showed an existence of a symmetry barrier which was thought to be an origin of the long lifetime of the intermediate.

SCHEME 1

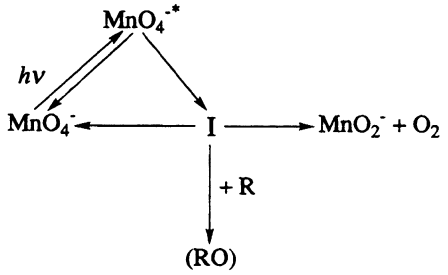

Despite these experimental studies, there still remain some ambiguous points in this decomposition reactions: for example, the origin of the wavelength and temperature dependencies of the quantum yield, the nature and the structure of the intermediate, etc. The purpose of this study is to clarify theoretically the essential aspects of the electronic processes of the photodecomposition reaction of the permanganate ion. We examine the electronic structures and the potential curves of the ground and excited states of the MnO_4^- ion along the assumed reaction pathway. We use the symmetry-adapted cluster[5] (SAC)/SAC−configuration interaction[6] (SAC-CI) method, which has been shown to be very useful for studying excited and ionized states of various molecules. A review was given in ref 7. In particular, it has been applied to the metal complexes like $MoO_{4-n}S_n^{2-}$ (ref 8), RuO_4, OsO_4 (ref 9), $TiCl_4$, $TiBr_4$, TiI_4 (ref 10), MnO_4^- (ref 11), CrO_2Cl_2 (ref 12), and CrO_4^{2-} (ref 13). We have previously clarified the nature of the excited states involved in the electronic spectrum of the MnO_4^- ion and compared it with the other calculational results.[11a] We have also given some preliminary results of the present subject.[11b] Furthermore, the SAC/SAC-CI method has been successful to calculate the potential energy curves of the ground and excited states of molecules such as Li_2 (ref 14), CO (ref 15), Ar_2 (ref 16), CeNe,

† Also from the Institute for Fundamental Chemistry, 34-4, Tankano-Nishihiraki-cho, Sakyo-ku, Kyoto 606, Japan.

⊗ Abstract published in *Advance ACS Abstracts,* May 1, 1995.

0022-3654/95/2099-8550$09.00/0

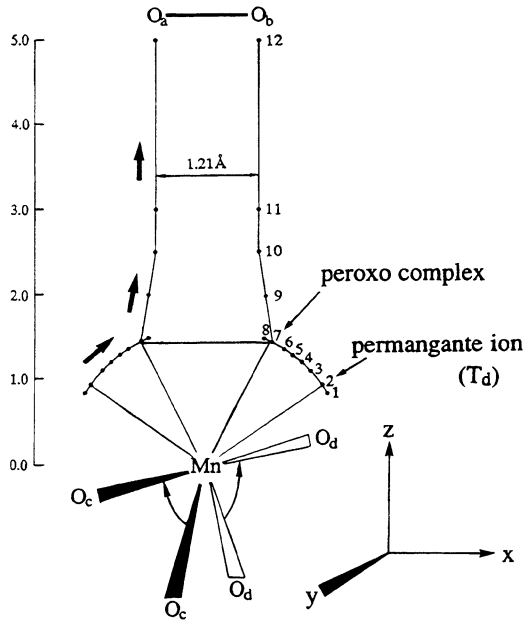

Figure 1. Assumed reaction pathway for the decomposition of the permanganate ion into MnO_2 and O_2.

CeAr, CeKr, CeXe (ref 17), O_2^-, and O_2^{2-} (ref 18) and surface–molecule interaction systems such as Pd_n-H_2 (ref 19), Pt_n-H_2 (ref 20), Ag_n-O_2 (ref 21), and $(alkali)_n-Cl_2$ (ref 22).

II. Calculational Details

This study is based on the *ab initio* molecular orbital theory. The Gaussian basis for the Mn atom is (5s5p5d)/[4s3p2d] set and the Ne core is replaced by the effective core potential.[23] For oxygen, we use (9s5p)/[4s2p] set of Huzinaga–Dunning[24] augmented by the diffuse s, p functions of $\alpha = 0.059$ (anion basis),[25] which is very important for the reaction involving oxygen anions species.[18,21]

The potential energy curves of the ground and excited states are calculated by the SAC/SAC-CI method. The active space consists of 12 higher occupied orbitals, which are mainly made of the 3d orbitals of Mn and the 2p orbitals of O, and 29 lower unoccupied orbitals calculated by the Hartree–Fock (HF) method. The configuration selections[26] are performed with the threshold of 5×10^{-5} and 1×10^{-4} hartree for the ground- and excited-state calculations, respectively. The HF calculations are carried out with the use of the program HONDO7[27] and the SAC/SAC-CI calculations with the program SAC85.[28]

In the photodecomposition of MnO_4^-, only molecular oxygen is generated, and no atomic oxygen is involved. We therefore assume the reaction pathway, as shown in Figure 1, where the Mn–O bonds do not break until the O–O bond is formed. O_a and O_b form an oxygen molecule and dissociate from the O_c–Mn–O_d system, keeping the C_{2v} symmetry. O_a and O_b are located on the xz-plane and O_c and O_d on the yz-plane. The Mn atom is located at the origin.

From 1 to 8, only the O_a-Mn-O_b angle changes from 119° to 49°, keeping the Mn–O_a and Mn–O_b distances at 1.629 Å, which is the equilibrium distance of the MnO_4^- ion.[29] 2 corresponds to the equilibrium geometry of MnO_4^-. The O_c and O_d atoms do not move and the O_c-Mn-O_d angle is kept at the T_d angle. From 7 to 12, the distance between the Mn atom and the O_a-O_b bond changes from 1.45 to 5.00 Å. At 9, the O_a-O_b distance and the O_c-Mn-O_d angle are 1.35 Å and 140°, respectively. They are fixed at 1.21 Å and 180°, respectively, for the points from 10 to 12. The Mn-O_c and Mn-O_d distances are fixed at 1.629 Å throughout the reaction pathway. We further optimize the geometries at several key points for the ground and lowest excited states in the HF/SE-CI level and examine the reliability of the assumed reaction pathway in Appendix C.

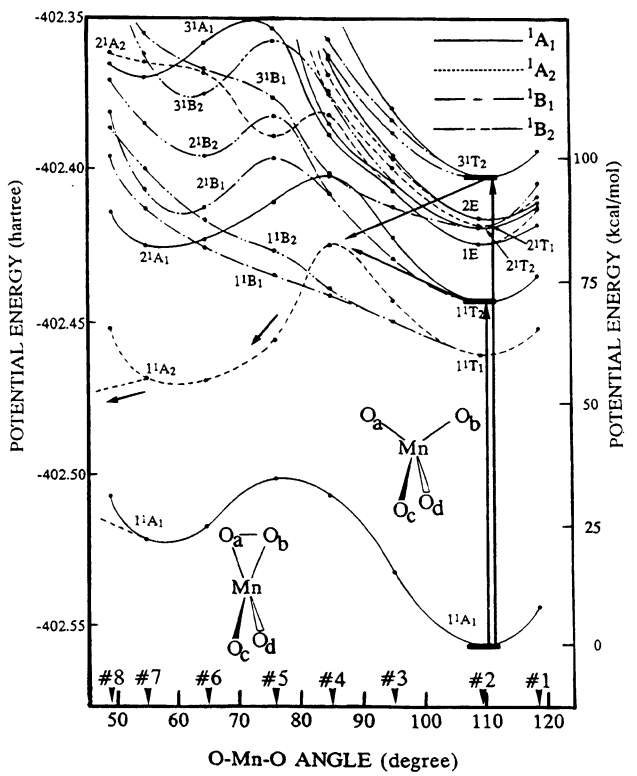

Figure 2. Potential energy curves of the ground and excited states of MnO_4^- calculated by the SAC/SAC-CI method for the reaction pathway shown in Figure 1. The arrows show the photochemical reaction route. The energy scale on the right-hand side is in kcal/mol relative to the energy of the ground state of the T_d permanganate ion.

III. Results and Discussions

The photochemical reaction of MnO_4^- starts from the absorption of light at the equilibrium tetrahedral structure. In the previous paper,[11] we have calculated the electronic excitation spectrum of MnO_4^- by the SAC/SAC-CI method. We have assigned the four observed bands to the allowed transitions to the $^1T_2$ states.[11] We note that the calculated oscillator strength of the second band is much smaller than those of the first and third bands, and this tendency agrees with the experimental one. In the photochemical reaction, therefore, the transition probability to the 2^1T_2 state is much smaller than those to the 1^1T_2 and 3^1T_2 states. The absorptions at 546 nm (2.27 eV) and 311 nm (3.99 eV), both of which induce the decomposition reaction, correspond to the excitations to the 1^1T_2 and 3^1T_2 states, respectively. The measurement of quantum yields used light with a wavelength between 254 nm (4.88 eV) and 578 nm (2.15 eV),[2] so that excitations to the 4^1T_2 and higher states were not involved in his experiment. Figure 2 shows the potential energy curves of the ground and excited states in the bending process from 1 to 8. The excitations to the 1^1T_2 and 3^1T_2 states are shown by the arrows at 2 in Figure 2.

The photoexcited ion in the 1^1T_2 and 3^1T_2 states would be relaxed with or without radiation. Relaxation to the $^1A_1$ ground state, which gives the starting complex, with radiation may be observed by fluorescence experiments. On the other hand, the radiationless internal conversion occurs by coupling several vibrational modes, whose probability from the state Ψ_1 to Ψ_2 is given by

$$\langle \Psi_2 | d/dQ | \Psi_1 \rangle$$

where **Q** is one of the vibrational modes. Of course, the selection rule of this transition is different from that of the dipole transition. Roughly speaking, the probability of the internal conversion is larger as the energy levels between the two states are closer, because of the Franck–Condon factor. Figure 2 shows that the potential energy curves of the excited states are rather crowded, though a large gap of 40–60 kcal/mol exists between the ground and the lowest excited states. Therefore, the vertically excited 1^1T_2 and 3^1T_2 states at the T_d structure would be relaxed to the 1^1T_1 (1^1A_2) state after several internal conversions among the excited states, as the Kasha rule implies. It is noted that direct transitions from the 1^1T_2 and 3^1T_2 to the 1^1T_1 (1^1A_2) states do not necessarily occur.

The 1^1A_2 state is connected with the 1^1T_1 state, when the symmetry of the ion changes from T_d to C_{2v}. At the 1^1A_2 state, the potential energy at position 7 is lower than that at 2, namely, the permanganate ion. In Figure 2, the potential minimum of the 1^1A_2 state around 7 is artificial, since there is another path leading to the dissociation as shown in Figure 1 and as will be discussed later. When the excited ion is relaxed to the 1^1A_2 state, it is easy to change its geometry from the T_d structure to the C_{2v} one, and further to the separated system, which will be explained later.

Along the 1^1A_2 state, there is a potential barrier at position 4. The energy of the 1^1T_2 state at the vertical geometry 2 is lower than the top of the barrier, but that of the 3^1T_2 state is higher. When the internal conversion starts from the 1^1T_2 state, the process needs to go over the barrier so that the reaction rate would depend on the temperature despite the photochemical process. This is actually observed for the reaction starting from 546-nm light. On the other hand, when the reaction starts from the 3^1T_2 state, the sysem has sufficient energy for going over the barrier. This difference is a factor for the wavelength dependence of the quantum yield; that is, the quantum yield for the shorter wavelength is much larger than that for the longer one.

Figure 3 shows the energy diagram for the photochemical reaction of MnO_4^- calculated by the present study. The potential energies of the separated systems, $MnO_2 + O_2^-$ and $MnO_2^- + O_2$, are calculated by using the SAC-CI method and the experimental values. The energies of MnO_2 and MnO_2^- are due to the SAC/SAC-CI method and the energy levels of O_2 and O_2^- are due to the SAC-CI calculation of O_2^- and the experimental electron affinity of O_2[30] and the experimental energy difference between the $^3\Sigma_g^-$ and $^1\Delta_g$ states.[31]

The stable geometries of MnO_2 and MnO_2^- are both linear, and the ground states are $^2\Delta_g$ and $^3\Delta_g$, respectively. Since the energy difference between $O_2 + MnO_2^-$ and $O_2^- + MnO_2$ is about 80 kcal/mol and the energy level of the latter is higher than those of the 1^1T_2 and 3^1T_2 states of the T_d permanganate ion, the former is the product of the decomposition reaction of MnO_4^-. This result agrees with the ESR experiment by Kläning *et al.*[3]

The $^3\Delta_g$ and $^1\Sigma_g^+$ states of MnO_2^- correspond to the configurations $(3d)^9(4s)^1$ and $(3d)^{10}(4s)^0$ of Mn, respectively. Figure 4 shows the schematic orbital correlation diagram for the interaction of O_2 and MnO_2^- in the C_{2v} peroxo MnO_4^- complex, which corresponds in Figure 2 to the potential minumum at 7 of the $^1A_1$ ground state. The left-hand side shows the MO's of the $^3\Sigma_g^-$ state of O_2, and the right-hand side those of the $^3\Delta_g$ state (ground state) of linear MnO_2^-. In the peroxo complex, MnO_2^- and O_2 are stabilized mainly by the two interactions as illustrated in Figure 4; one is the interaction

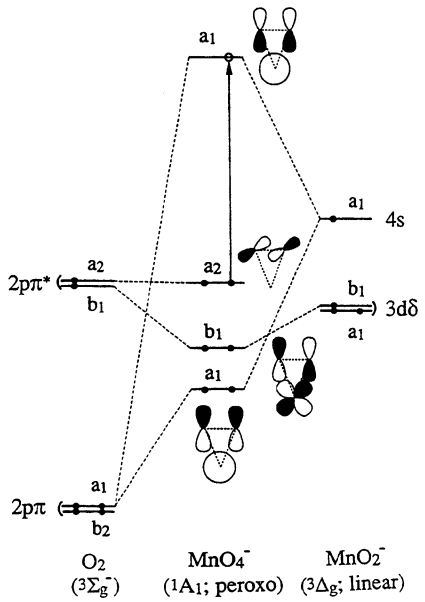

Figure 3. Energy diagram for the photochemical reaction of MnO_4^- calculated by the SAC/SAC-CI method.

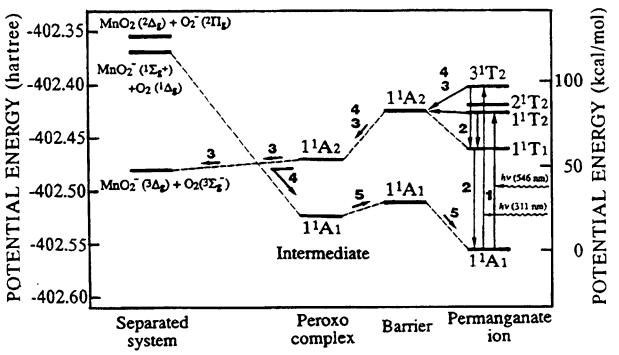

Figure 4. Orbital correlation diagram for the interaction of MnO_2^- and O_2 in the peroxo MnO_4^- complex. The left-hand side shows the active MO's of the ground $^3\Sigma_g^-$ state of O_2 and the right-hand side those of the ground $^3\Delta_g$ state of the linear MnO_2^-.

between the in-plane π^* orbital of O_2 and the $3d_{xz}$ orbital of Mn and the other is the interaction between the in-plane π orbital of O_2 and the 4s orbital of Mn. The O–O distance of this complex is about 1.5 Å, which is longer than the equilibrium distances of O_2^- and O_2, namely, 1.35 and 1.21 Å, respectively.[21] The O–O bond in this complex has only one σ bond because of the full occupation of the π^* orbitals of O_2, as shown in Figure 4. In this sense, this state corresponds to the peroxo (O_2^{2-}) complex.

Figure 4 indicates that the decomposition reaction from the $^1A_1$ ground state of the peroxo complex leads to MnO_2^- ($^1\Sigma_g^+$) + O_2 ($^1\Delta_g$), which is the excited state, about 70 kcal/mol higher than the ground state. As shown in Figure 3, it is about 90 kcal/mol higher than the $^1A_1$ ground states of the peroxo complex. On the other hand, the reaction from the $^1A_2$ excited state, which is generated by the one-electron excitation from the out-of-plane π^* orbital of O_2 to the antibonding MO between MnO_2^- and O_2, as shown by the arrow in Figure 4, leads to MnO_2^- ($^3\Delta_g^+$) + O_2 ($^3\Sigma_g^-$), which is the ground state. This shows that the photochemical and thermal decomposition reactions of MnO_4^- are symmetry allowed and forbidden, respectively. As seen from Figure 3, the energy level of the ground state of the separated system is lower than that of the 1^1A_2 state of the peroxo complex and there is no potential barrier between them. The potential energy curves for the dissociation

process from 7 to 12 are calculated by the full CI method within the small active space, which is shown in the Appendix. Thus, the photodecomposition reaction of MnO_4^- occurs smoothly from the $^1A_2$ excited state of the peroxo complex leading to the ground-state product, $MnO_2^-(^3\Delta_g^+) + O_2(^3\Sigma_g^-)$.

The quenching of the photoexcited ion, which decreases the quantum yield of the photochemical reaction, gives two different complexes. Namely, when the quenching occurs at the positions from 1 to 5, the T_d permanganate ion will be the product. When it occurs at the positions from 5 to 7, the peroxo complex will be generated. The energy emitted for giving the peroxo complex is smaller than that for giving the permanganate ion, as shown in Figure 2. It is interesting if we can observe the fluorescence of the photoexcited MnO_4^- ion experimentally, though the intensity should be small because of the dipole-forbidden transition.

As shown in Figure 3, the potential energy curves of the 1^1A_1 and 1^1A_2 states cross each other along the dissociation process. Therefore, the internal conversion from the 1^1A_2 to 1^1A_1 states may occur through this crossing point. This conversion also leads to the ground state of the peroxo complex, which is the intermediate proposed by Lee *et al.*[4]

The peroxo complex in the ground state may transform back to the permanganate ion. In this transformation, the two MO's with the symmetries of a_1 and b_1 exchange between occupied and unoccupied spaces. The a_1 orbital has a O−O σ-bonding character and, therefore, becomes more stable as the O−O distance is shortened. On the other hand, the b_1 orbital, having a O−O σ-antibonding character, becomes less stable, but at the T_d geometry it contributes to the Mn−O bond. The potential barrier in this transformation is thus due to the Woodward-Hoffmann symmetry-forbidden nature as pointed our by Lee *et al*,[4] though the barrier height is comparatively small, as calculated to be 13 kcal/mol by the SAC method. This is the origin of the long life time of the intermediate, which is indicated experimentally.[4]

As a summary of the present study, we propose Scheme 2 for the photochemical reaction of MnO_4^-. Arabic numbers in this scheme correspond to the processes in the energy diagram of Figure 3. Process 1 is the absorption of light at the T_d structure. The quenching of the photoexcited states at the T_d structure is process 2. The relaxation along the excited-state potential curve of the 1^1A_2 state, which directly leads to the decomposition giving the ground-state MnO_2^- and O_2, is shown by 3. Process 4 is relaxation along the 1^1A_2 excited state and internal conversion to the 1^1A_1 ground state, which gives the peroxo complex considered to be the intermediate. Process 5 is the transformation of the intermediate back to the permanganate ion.

Based on the experimental observations, Lee *et al.*[4] have proposed Scheme 1, which involves the formation of the intermediate. The present Scheme 2 confirms the validity of their Scheme 1, except for the decomposition process 3. They considered that the decomposition into $MnO_2^- + O_2$ occurs from the intermediate, while the present study shows that it occurs directly from the photoexcited state.

IV. Concluding Remarks

In the present study, we have tried to clarify the electronic mechanism of the photodecomposition reaction of MnO_4^- by the *ab initio* theory including electron correlations. The SAC/SAC-CI method has been applied to the calculations of the potential energy curves for the ground and excited states of the permanganate ion along the reaction pathway.

The 546- and 311-nm absorption bands, which lead to the photochemical decomposition reaction, correspond to the dipole-allowed transitions to the 1^1T_2 and 3^1T_2 states, respectively. The first excited state of the peroxo complex, the 1^1A_2 state, plays a key role in the reaction. Along the potential energy curve of the 1^1A_2 state, the photoexcited state directly dissociates into the ground state of the separated system: $MnO_2^-(^3\Delta_g^+) + O_2(^3\Sigma_g^-)$. We think that the energy barrier in the 1^1A_2 state causes the strong wavelength dependence of the quantum yield and the slight temperature dependence for the light at the longer wavelength. The present study shows that the photochemical and thermal decomposition reactions of MnO_4^- are symmetry allowed and forbidden, respectively.

SCHEME 2

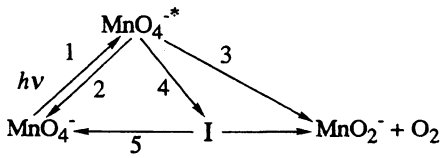

The photoexcited 1^1A_2 state potential curve of MnO_4^- crosses the $^1A_1$ ground-state curve after taking the geometry of the peroxo complex, and therefore the energy relaxation would easily occur through this crossing. The ground-state ($^1A_1$) peroxo complex thus generated corresponds to the intermediate observed by the experiment.[4] There is a potential barrier between the C_{2v} peroxo complex and the T_d permanganate ion, which is due to the avoided crossing of the two $^1A_1$ states, and a symmetry barrier as explained by Lee *et al.*[4] This barrier gives a long life time to the peroxo complex intermediate.

The electronic mechanism proposed by the present *ab initio* study, which is shown by Scheme 2, consistently explains the previous experimental results for the photochemical decomposition reaction of MnO_4^-.

Acknowledgment. The calculations have been carried out with the computers at the Data Processing Center of Kyoto University and at the Institute for Molecular Science. Part of this study has been supported by the Grant-in-Aid for Scientific Research from the Japanese Ministry of Education, Science, and Culture, and by CIBA-GEIGY Foundation (Japan) for the Promotion of Science.

Appendix A: Comparison between the HF and the SAC Results

Here, we compare the HF and the SAC results for the MnO_4^- ion. Figure 5 shows the potential energy curve of the ground state of MnO_4^- from 1 to 9 on the reaction pathway shown in Figure 1. The upper curve is calculated by the HF method and the lower one by the SAC method. Both HF and SAC calculations give two minima corresponding to the T_d permanganate ion and the peroxo complex.

The HF calculation shows that the peroxo complex is more stable than the T_d permanganate complex by 43 kcal/mol. That is not consistent with the experimental fact that the equilibrium geometry of MnO_4^- is tetrahedral. On the other hand, the SAC calculation correctly shows that the permanganate structure is more stable by 21 kcal/mol, which is consistent with the experimental fact. This result clearly shows that electron correlations are quite important even for a qualitative description of the equilibrium geometry of MnO_4^-.

The potential barrier between the permanganate and the peroxo complexes is due to the avoided crossing of the two $^1A_1$ states and corresponds to the symmetry barrier as mentioned above. Since the HF method cannot well describe this avoided crossing, the potential curve of the HF calculations has a cusp

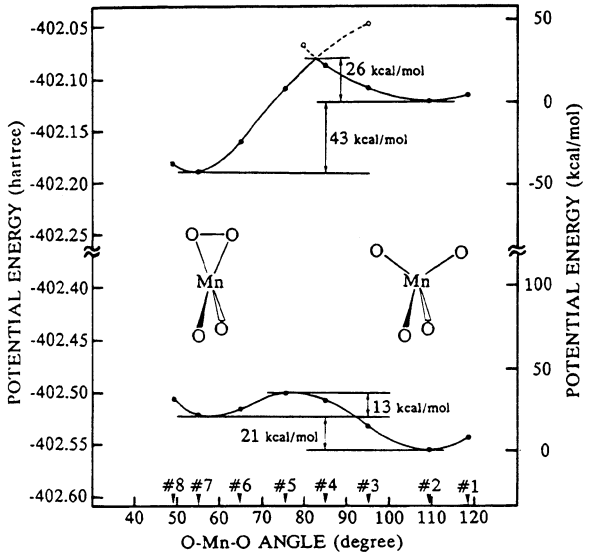

Figure 5. Potential energy curves of the ground state of the MnO_4^- calculated by the HF and SAC methods for the reaction pathway shown in Figure 1.

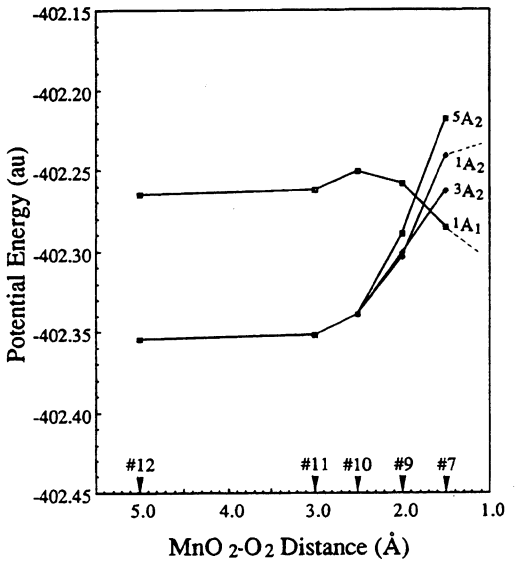

Figure 6. Potential energy curves of the lowest singlet, triplet, and quintet states of MnO_4^- calculated by the CI method for the dissociation process from 7 to 12 shown in Figure 1.

at the barrier. On the other hand, the SAC method gives a natural description of the potential curve.

Appendix B: Potential Energy Curves for the Dissociation Process

The potential energy curves of the lower singlet, triplet, and quintet states are calculated for the dissociation process from 7 to 12 by the CI method, which is shown in Figure 6. In the CI calculations, single, double, triple, and quadruple excitations are considered within the small active space of [12 × 2], which corresponds to the full excitations. The CI calculations are carried out with the use of the program HONDO7.[18]

In this dissociation process, the ground state changes from the closed-shell $^1A_1$ state to the open-shell A_2 state. The 1^1A_1 curve has a barrier around the Mn−O_2 distance of 2.5 Å. On the other hand, all the A_2 curves are repulsive, namely, there are no barriers in the states. The singlet, triplet, and quintet A_2 curves overlap in the range of Mn−O_2 distance from 2.5 to 5.0 Å. This state corresponds to the ground state of the separated system, namely, the $^3\Delta_g$ state of MnO_2^- plus the $^3\Sigma_g^-$ state of O_2.

Appendix C: Reliability of the Assumed Reaction Pathway

We have assumed the reaction pathway shown in Figure 1 for the photodecomposition reaction of MnO_4^-. In the actual system, all the atoms should move, and therefore, we examine here the reliability of the assumed reaction pathway by optimizing the geometries of the 1^1A_1 ground and 1^1A_2 excited states by the HF/SE-CI method at several key positions. In particular, we investigate the effect of relaxing the geometries of the opposite O atoms, O_c and O_d.

Table 1 shows the assumed and optimized geometries and their energies at positions 2, 4, 7, 9, and 10. Positions 2, 4, and 7 correspond to the permanganate, barrier, and peroxo complex, respectively, as mentioned above. For the T_d permanganate ion, the optimized Mn−O distance in the 1^1A_1 state is 1.564 Å in comparison with the experimental value of 1.629 Å.[29] The energy difference between the experimental and optimized Mn−O distances is 8.1 kcal/mol. As is well-known, the HF calculation underestimates the bond distance. For the 1^1A_2 excited state, the assumed geometries do not deviate much

TABLE 1: Optimized Geometries and Corresponding Energies in the HF/SE-CI Level at Positions 2, 4, 7, 9 and 10[a]

	distance, Å		angle, deg		energy	
state	Mn-$O_{a,b}$	Mn-$O_{c,d}$	O_a-Mn-O_b	O_c-Mn-O_d	E, au	ΔE,[b] kcal/mol
2 (permanganate)						
1^1A_1 (fix)	1.629	1.629	109.5	109.5	−402.120 249	0.00
1^1A_1 (opt)	1.564*	1.564*	109.5	109.5	−402.133 188	−8.11
4 (barrier)						
1^1A_2 (fix)	1.629	1.629	109.5	109.5	−401.990 323	0.00
1^1A_2 (opt)	1.629	1.864*	109.5	97.9*	−402.008 858	−11.62
7 (peroxo)						
1^1A_2 (fix)	1.629	1.629	109.5	109.5	−402.181 919	0.00
1^1A_2 (opt)	1.629	1.578*	109.5	115.5*	−402.188 236	−3.96

	distance, Å			angle, deg	energy	
state	Mn-O_2	O_a-O_b	Mn-$O_{c,d}$	O_c-Mn-O_d	E, au	ΔE,[b] kcal/mol
9						
1^1A_2 (fix)	2.000	1.350	1.629	140.0	−402.163 981	0.00
1^1A_2 (opt)	2.000	1.350	1.590*	117.5*	−402.175 569	−7.27
10						
1^1A_2 (fix)	2.500	1.210	1.629	180.0	−402.177 355	0.00
1^1A_2 (opt)	2.500	1.210	1.659*	180.0*	−402.180 069	−1.70

[a] Optimized geometries are marked by the asterisks. [b] Energy difference between the fixed and optimized geometries.

from the optimized geometries at 4, 7, 9, and 10, respectively. It is noted that the O_c-Mn-O_d angle of the assumed pathway at 10 agrees with the optimized one of 180.0°.

We next consider the effects of the geometry optimization summarized in Table 1 on the energy profiles given in Figures 2 and 3 and, therefore, on the mechanism of the photodecomposition reaction of MnO_4^-. We assume the energy shifts at the HF/SE-CI level are similar to those at the SAC/SAC-CI level. Using the optimized geometry at 4, the energy barrier becomes smaller but still remains higher than the energy level of the 1^1T_2 state at 2. The behavior of the 1^1A_2 curve, which goes down monotonically from 4 to 10, does not change with the optimized geometries. We therefore believe that the mechanism presented in this study would remain unaltered even by using the fully-optimized reaction pathway.

References and Notes

(1) Mathews, J. H.; Dewey, L. H. *J. Phys. Chem.* **1913**, *17*, 211.
(2) Zimmerman, G. *J. Chem. Phys.* **1955**, *23*, 825.
(3) Kläning, U.; Symons, M. C. R. *J. Chem. Soc.* **1959**, 3269.
(4) Lee, D. G.; Moylan, C. R.; Hayashi, T.; Brauman, J. I. *J. Am. Chem. Soc.* **1987**, *109*, 3003.
(5) Nakatsuji, H.; Hirao, K. *J. Chem. Phys.* **1978**, *68*, 2035.
(6) Nakatsuji, H. *Chem. Phys. Lett.* **1978**, *59*, 362; **1979**, *67*, 329, 334.
(7) Nakatsuji, H. *Acta Chim. Hung.* **1992**, *129*, 719.
(8) Nakatsuji, H.; Saito, S. *Int. J. Quantum Chem.* **1991**, *39*, 93.
(9) Nakatsuji, H.; Saito, S. *J. Chem. Phys.* **1990**, *93*, 1865.
(10) Nakatsuji, H.; Ehara, M.; Palmer, M. H.; Guest, M. F. *J. Chem. Phys.* **1992**, *87*, 2561.
(11) (a) Nakai, H.; Ohmori, Y.; Nakatsuji, H. *J. Chem. Phys.* **1991**, *95*, 8287. (b) Nakai, H.; Nakatsuji, H. *J. Mol. Struct. THEOCHEM* **1994**, *311*, 141.
(12) Yasuda, K.; Nakatsuji, H. *J. Chem. Phys.* **1993**, *99*, 1945.
(13) Jitsuhiro, S.; Nakai, H.; Hada, M.; Nakatsuji, H. *J. Chem. Phys.* **1994**, *101*, 1029.
(14) Nakatsuji, H.; Ushio, J.; Yonezawa, T. *Can. J. Chem.* **1985**, *63*, 1857.
(15) Kitao, O.; Nakatsuji, H. *Proc.-Indian Acad. Sci.* **1986**, *96*, 155.
(16) Mizukami, Y.; Nakatsuji, H. *J. Chem. Phys.* **1990**, *92*, 6084.
(17) Nakatsuji, H.; Ehara, M. *Chem. Phys. Lett.* **1990**, *172*, 261.
(18) Nakatsuji, H.; Nakai, H. *Chem. Phys. Lett.* **1992**, *197*, 339.
(19) Nakatsuji, H.; Hada, M. *J. Am. Chem. Soc.* **1985**, *107*, 8264; Nakatsuji, H.; Hada, M.; Yonezawa, T. *J. Am. Chem. Soc.* **1987**, *109*, 1902.
(20) Nakatsuji, H.; Matsuzaki, Y.; Yonezawa, T. *J. Chem. Phys.* **1988**, *88*, 5759.
(21) Nakatsuji, H.; Nakai, H. *Chem. Phys. Lett.* **1990**, *174*, 283; *J. Chem. Phys.* **1993**, *98*, 2423.
(22) Nakatsuji, H.; Kuwano, R.; Morita, H.; Nakai, H. *J. Mol. Catal.* **1993**, *82*, 221.
(23) Hay, P. J.; Wadt, W. R. *J. Chem. Phys.* **1985**, *82*, 299.
(24) Huzinaga, S. *J. Chem. Phys.* **1965**, *42*, 1293; Dunning, T. H., Jr. *J. Chem. Phys.* **1970**, *53*, 2823.
(25) Dunning, T. H., Jr.; Hay, P. J. *Modern Theoretical Chemistry*; Schaeffer, H. F., III, Eds.; Plenum: New York, 1977; Vol. 3.
(26) Nakatsuji, H. *Chem. Phys.* **1983**, *75*, 425.
(27) Dupuis, M.; Watts, J. D.; Viller, H. O.; Hurst, G. J. B. Program Library HONDO7 No. 1501, Computer Center of the Institute for Molecular Science, 1989.
(28) Nakatsuji, H. Program System for SAC and SAC-CI calculations; Program Library No. 146 (Y4/SAC); Data Processing Center of Kyoto University, 1985; Program Library SAC85, No. 1396; Computer Center of the Institute for Molecular Science, 1981.
(29) Palenik, G. J. *Inorg. Chem.* **1967**, *6*, 503.
(30) Huber, K. P.; Herzberg, G. *Molecular Spectra and Molecular Structure, IV. Constants of Diatomic Molecules*; Van Nostrand Reinhold: New York, 1979.
(31) Celotta, R. J.; Bennett, R. A.; Hall, J. L.; Siegel, M. W.; Levine, J. *Phys. Rev.* **1972**, *A6*, 607.

JP942995B